

MORPHOLOGY OF *SPITZER* 24 μ M-DETECTED GALAXIES IN THE UDF: THE LINKS BETWEEN THE STAR FORMATION AND GALAXY MORPHOLOGY

Y. SHI, G. H. RIEKE, C. PAPOVICH, P. G. PÉREZ-GONZÁLEZ, E. LE FLOC'H

Draft version July 5, 2018

ABSTRACT

We have studied the morphologies of luminous infrared galaxies (LIRGs; $L_{IR}(8-1000\mu\text{m}) > 10^{11}L_{\odot}$) at $0.3 \leq z < 1.4$ in the *HST* Ultradeep Field (UDF) by calculating concentration and asymmetry indices and comparing the results with similar calculations for: (1) galaxies at similar redshift that are less infrared-active; and (2) local LIRGs. We find that the high-redshift samples are dominated by galaxies with concentrations similar to local late-type disk galaxies; however, they are significantly more asymmetric than most local galaxies but are similar in both regards to local LIRGs. On average, the high-redshift infrared-active galaxies are slightly more asymmetric than the less-active ones, although they do include a significantly higher portion of highly asymmetric (merging?) systems and a lower portion of more concentrated, symmetric ones. The morphological similarity of infrared-active and typical infrared-inactive galaxies at high-redshift suggests that they may be from the same parent population, but are in different stages of an episodic star formation process. The similarity between high-redshift and local LIRGs suggests that a certain level of asymmetry is generally associated with LIRG-level activity.

Subject headings: galaxies: interactions — infrared: galaxies

1. INTRODUCTION

Two fundamental aspects of galaxy formation and evolution are mass assembly and morphology transformation. While mass assembly is often accompanied by strong episodes of star formation, the morphology of a galaxy reflects its dynamical history and evolution. For example, different Hubble types are associated with different motion patterns of stars and gas and different histories of star formation. The interplay between these two processes may play a crucial role in galaxy formation and evolution: the dynamics, indicated by the morphology, drives the star formation, while the depletion of gas from star formation as well as feedback from young stars through supernovae and stellar winds may re-shape the galaxy morphology. Thus, in the local Universe, later-type galaxies are gas-rich and the sites of elevated star formation (for a review, see Kennicutt 1998), while the more extreme star-forming galaxies often show peculiar morphologies, resulting from collisions and mergers (e.g. Soifer et al. 1984; Cutri & McAlary 1985; Sanders et al. 1988; Armus et al. 1987; Kleinmann et al. 1988; Barton et al. 2000).

The comoving star formation density rises by an order of magnitude from $z = 0$ to $z \sim 1$ (Lilly et al. 1995; Ellis et al. 1996; Steidel et al. 1999; Hopkins 2004). In the high-redshift universe, the high rate of star formation seems to be associated with a large fraction of peculiar and morphologically disturbed galaxies. Deep surveys, especially those carried out by the Hubble Space Telescope (*HST*), reveal that the fraction of irregular and interacting galaxies increases dramatically toward high redshift, from around 4% (Marzke et al. 1998) in the local universe to more than 80% at $z \geq 2$ (Conselice et al. 2005). Even the high-redshift galaxies classified as traditional Hubble types still show many peculiar features,

with tidal or disturbed structures and distorted disks. However, Melbourne et al. (2005) study the optical morphology evolution of LIRGs, finding that peculiar-to-spiral LIRG fraction increases at lower redshift. Our goal in this paper is to probe how the star formation and galaxy morphology are linked out to $z \sim 1$.

The Hubble (1926, 1936) galaxy classification as modified by Sandage (1961), Sandage & Tammann (1987), Sandage & Bedke (1994), van den Bergh (1960a,b) and de Vaucouleurs (1959), has achieved remarkable success in categorizing local galaxies with normal morphology (for a review, see Roberts & Haynes 1994). However, the Hubble scheme has a single class for peculiar morphologies and thus is unable to reflect the vast variations within this category. It is therefore inadequate to classify the morphologies of high-redshift galaxies using the local Hubble sequence, because a significant fraction of the population are irregular galaxies or normal galaxies but with perturbed features (Driver et al. 1995, 1998; Abraham et al. 1996a,b; Brinchmann et al. 1998; Cassata et al. 2005). A different classification method, called the *CA* system, is particularly useful for peculiar galaxies at high redshift. It is based on morphological parameters: the light concentration index, C (Okamura et al. 1984; Abraham et al. 1994; Bershady et al. 2000; Conselice 2003), and the asymmetry index, A , first introduced by Abraham et al. (1994) and developed by Conselice et al. (2000). Its primary virtues are that it is objective and can be applied consistently to low resolution and low signal-to-noise images. The success in distinguishing between different Hubble types; the robust measurements of parameters over a large range of redshift range of galaxy types especially quantifying the irregularity of peculiar galaxies; and the strong relations between the parameters and physical properties such as color, all make the *CA* system useful for classifying galaxies found in deep fields.

Out to $z \sim 1.5$, the star formation density is dominated

arXiv:astro-ph/0603453v1 17 Mar 2006

by LIRGs (Le Floch et al. 2005; Pérez-González et al. 2005). Studies of the morphologies of these high-redshift LIRGs are necessary to understand how morphologies and star formation are coupled to drive galaxy evolution. In this paper, we utilize a Multiband Imaging Photometer (MIPS; Rieke et al. 2004) deep survey of the *HST* Ultra-deep Field (UDF). The extremely deep *HST* images in the UDF allow us to apply the *CA* system to analyze the optical morphologies of the LIRGs in the MIPS survey even including faint features with low optical surface brightness.

The morphologies of galaxies in the UDF have been recently studied by Elmegreen et al. (2005) who mainly focus on the distribution of galaxy types and Menanteau et al. (2005) who study the contribution of various types of galaxies to the cosmic star formation rate (SFR). The detailed analysis of the morphologies of the high-redshift LIRGs and the comparisons to other MIPS-non-detected galaxies and local LIRGs in this paper complement these studies and enable us to gain new insight to the following questions: How do the intensely star-forming galaxies at $z \sim 1$ relate to other galaxies at the same epoch? How are star formation and galaxy morphologies coupled to drive galaxy evolution?

In this paper, we measure the concentration and asymmetry indices from the *HST* images to quantify the morphologies of the sample of high-redshift LIRGs in the UDF, of a comparison sample of MIPS-non-detected galaxies in the UDF, and of a local sample of LIRGs. In § 2, we summarize the observations, data reduction, and band merging. In Section § 3, we describe the selection of the samples and the measurement of the structural parameters. In § 4, we present the morphological characteristics of the galaxies. In Section § 5, we discuss the implications for high-redshift galaxy evolution based on the results from the preceding section. In § 6, we present our conclusions. Throughout this paper, we assume $H_0=70$ km s⁻¹ Mpc⁻¹, $\Omega_0=0.3$ and $\Omega_\Lambda=0.7$. We use AB magnitudes throughout, where $m_{AB} = 23.9 - 2.5 \log(f_\nu / 1 \mu\text{Jy})$. We denote magnitudes from the *HST* ACS passbands F435W, F606W, F775W, and F850LP as B_{435} , V_{606} , i_{775} , and z_{850} , respectively.

2. THE DATA

2.1. *Spitzer* Data

Our 24 μm MIPS (Rieke et al. 2004) observations of the UDF are part of a scan map covering a larger area centered on the Chandra Deep Field South (CDFs; Giacconi et al. 2002). The images were processed with the MIPS instrument team Data Analysis Tool (DAT; Gordon et al. 2005). Descriptions of 24 μm source detection and photometry are given by Papovich et al. (2004). Table 1 lists the sources detected at 24 μm with unambiguous optical counterparts that are the primary subject of this paper. The CDFS was also observed under GTO time with the Infrared Array Camera (IRAC) (Fazio et al. 2004) at 3.6, 4.5, 5.8 and 8.0 μm . Source detection and photometry were done with SExtractor (Bertin & Arnouts 1996) following similar procedures as in Huang et al. (2004).

2.2. *HST* Data

The UDF is a public *HST* survey to image a single Advanced Camera for Surveys (ACS) wide field cam-

era (WFC) field (11.5 arcmin²) in 4 broad-band filters (F435W; F606W; F775W; F850LP) (Beckwith et al. 2005). The WFC has a resolution of $\sim 0.12''$, corresponding to 540 pc at $z=0.3$ and 1 kpc at $z=1.0$. For our analysis we use the reduced UDF data v1.0 made public by the Space Telescope Science Institute (STScI) on 09 March 2004. The z -band-based catalog is used for optical identification of MIPS sources. A total of 7016 objects detected at z -band gives a source density of 0.169 arcsec⁻². The 10- σ limiting magnitudes at B -band, V -band, i -band and z -band are 28.7, 29.0, 29.0 and 28.4, respectively, in an aperture of 0.2 arcsec², corresponding to 10- σ surface brightness of 27.82, 28.12, 28.12 and 27.52 arcsec⁻², respectively.

We also use Near-Infrared Camera and Multi-Object Spectrometer (NICMOS) UDF Treasury Observations for the photometry data for our photo- z code. NICMOS UDF Observations use camera 3 with a resolution of 0.2''/pixel (1.6 kpc at $z=1$). Due to the small field of NICMOS camera, the NICMOS UDF only covers a subsection (5.76 arcmin²) of the optical UDF. The data reduction and photometry are given by Thompson et al. (2005). The catalog contains 1293 objects, giving a source density of 0.0624 arcsec⁻². The 5- σ limiting AB magnitude is 27.7 at 1.1 and 1.6 μm in a 0.6'' diameter aperture, corresponding to a surface brightness of 27.01 arcsec⁻².

2.3. Results and Band Merging

We identified 52 sources with 24 μm flux density greater than 0.06 mJy (at which level the completeness is $\sim 50\%$ in the UDF (Papovich et al. 2004)). We searched for ACS counterparts on the z -band image of the UDF within a 2.5''-radius circular region surrounding each 24 μm source. The choice of this search radius is motivated by the large FWHM of the MIPS 24 μm PSF ($\sim 6''$) and the positional accuracy at 24 μm ($\sim 0.5''$ rms). 2.5'' (10 kpc at $z=0.3$ and 20 kpc at $z=1.0$) is large enough to account for the possible physical shift between the locations of infrared emission and the optical emission observed in local interacting galaxies (e.g. Le Floch et al. 2002).

Multiple optical sources are present in the search circle for 41 of 52 MIPS sources. The IRAC images were used to identify the most probable optical counterpart for these 41 MIPS sources. In the UDF, there are a total of 312 objects in the IRAC 4.5 μm catalog with flux density greater than 1.6 μJy at 50% completeness. 23 of the 41 MIPS sources have such an IRAC counterpart within a 1.0'' radius. The probability of random spatial superposition of IRAC sources in a 1.0''-radius circular region is 2.3 %, which indicates a high probability that the IRAC counterparts are physically related to the MIPS sources. We also visually inspected the IRAC image of each source to check if there is nearby IRAC source which might contaminate the 24 μm emission. MIPS-15950, which is contaminated in this way, is excluded. The search radius to match optical counterparts for IRAC sources is 1.5'', motivated by similar reasons to those for the MIPS sources. 15 of 22 IRAC sources have only one optical source within the search radius, which should be the optical counterpart of the corresponding MIPS source. For the remaining 25 MIPS sources with possible multiple optical counterparts, if an optical object is brighter than

other optical objects within the same search circle by 4 magnitudes, this optical object was taken to be the optical counterpart of the MIPS source. This association is justified because IR-luminous galaxies tend to be associated with optically bright galaxies (Mann et al. 1997). On the other hand, the probability of random spatial superposition is an order of magnitude larger for 4-magnitude fainter objects. Based on the above series of steps for deconvolution of multiple objects in the $24\ \mu\text{m}$ beam, 16 of 52 MIPS sources may still have multiple optical counterparts. We do not use these 16 sources in our analysis to avoid their affecting the distribution of the morphologies of the MIPS-detected sources. Our final sample therefore consists of 35 MIPS-detected galaxies that have unambiguous identifications with ACS images.

An alternative method for evaluating interactions, "pairs statistics", would be strongly affected by the handling of sources with multiple possible counterparts. However, the CA analysis employed here measures the structure of the central image and hence to first order is independent of such effects. As a test, we recomputed the classification parameters including the objects with multiple identifications and using the brightest object as the optical counterpart. We found that the basic results were unchanged; the mean asymmetry of the MIPS-detected objects got slightly smaller but by only 0.03.

Eighteen of our sample of 35 MIPS sources have spectroscopic redshifts based on the VLT/FORS2 spectroscopy catalog (Vanzella et al. 2005) and VIMOS VLT Deep Survey (VVDS) v1.0 catalog (Le Fèvre et al. 2004). For the remaining 17 sources, we use photometric redshifts. The publicly available COMBO-17 survey of the CDFS provides photometric redshifts by means of 17-band photometry (Wolf et al. 2004). The typical photometric redshift accuracy is $\delta z/(1+z) < 0.02$ for galaxies with $m_R < 22$ and reaches 0.1 at $m_R \sim 24$, allowing the rest-frame absolute magnitude to be accurate within 0.1 for $m_R < 22$ and 0.5 mag for $m_R \sim 24$. We searched for COMBO-17 counterparts for each ACS source within a radius of 0.45 arcsec. Given a total of 63,501 COMBO-17 objects in a field of view $31.5' \times 30'$, the probability of random spatial superposition in a $0.45''$ -radius circular region is only 1.1%. We visually inspected the ACS image of each source to assure we matched the right COMBO-17 counterpart. Seven MIPS sources have X-ray emission based on the X-ray 1 MS catalog (Giacconi et al. 2002) and photometric redshifts given by W. Zheng et al. (2004). For the ACS counterpart of any MIPS source without redshifts from these sources, we used our own photo- z code (see Pérez-González et al. 2005) based on ACS, NICMOS and IRAC observations. We also used our code to compute the redshift for any ACS source with a COMBO-17 counterpart with $m_R > 22$. The main advantage of this photo- z code is it uses photometry over a longer wavelength baseline (including the $1.6\ \mu\text{m}$ bump) to obtain redshifts for galaxies up to $z \sim 3$, with accuracy of $\delta z/(1+z) < 0.1$. We inspected the fitting individually to assure our code gave a robust measurement of redshifts. Except for MIPS-5106, sources with multiple redshifts have consistent measurements of redshift. For this source, we use our redshift measurement since the $1.6\ \mu\text{m}$ stellar bump is obviously detected at the IRAC bands in the SED.

The K-corrections for the optical four-band data are

computed using codes based on the template spectra of galaxies in the Sloan Digital Sky Survey (SDSS; Blanton et al. 2003).

We used the ACS image that is closest to rest-frame B band to compute the structural parameters for the galaxies. Therefore the maximum redshift in our study is 1.4, beyond which the observed z -band is shorter than the rest-frame B -band. The advantages of classification using rest-frame optical bands and the importance of morphological K-corrections are discussed further in Windhorst et al. (2002) and Papovich et al. (2003).

To obtain accurate total far-infrared luminosities, it is necessary to have photometry over the whole range of infrared wavelengths. In this study, however it is enough to have a coarse estimate of the total infrared luminosity. We used the template spectra of starburst galaxies (with the current SFR much larger than the past-averaged SFR) published by Lagache et al. (2004) to get the $8\text{-}1000\ \mu\text{m}$ total infrared luminosity from the observed $24\ \mu\text{m}$ flux density. Due to the high sensitivity of MIPS, some MIPS-detected galaxies at low redshift are normal galaxies, not starbursts. For them, we used the appropriate template for galaxies with total IR emission fainter than $10^{10}\ L_{\odot}$ (where the threshold is computed from the starburst template). The average conversion factor from $\nu L_{\nu}(24\ \mu\text{m})$ to total infrared luminosity is 20 with a dispersion of up to 0.2 dex, indicating that our conversion should be accurate typically within a factor 2 or 3 (Papovich & Bell 2002; Le Floc'h et al. 2005), which is enough for the analysis in this paper.

3. METHODOLOGY

3.1. Sample Definition

We only computed the structural parameters for 34 of the 35 MIPS sources that have signal-to-noise (S/N) ratios better than 100 and half light radius $r_{50} > 5$ pixels at z band. High signal-to-noise ratio (SNR) and large size are required for robust measures of the asymmetry parameters (Conselice et al. 2000; Bershady et al. 2000). The deep exposure in the UDF thus allowed us to compute reliably structural parameters for a high fraction (97%) of MIPS-detected galaxies.

The members of our control sample are defined to be undetected at $24\ \mu\text{m}$ and (1) to lie $5''$ away from all MIPS sources; (2) to have half light radius $r_{50} > 5$ pixels at z band; (3) to have SNR better than 100 at z band; and (4) to have a COMBO-17 photometric redshift smaller than 1.4. The last condition is necessary for K-corrections and requires $m_z < 25$ (Wolf et al. 2004). The final sample is composed of 252 normal galaxies, representing 80% of the galaxies undetected at $24\ \mu\text{m}$ meeting only the first three requirements.

Our main goal is to investigate the morphologies of high-redshift LIRGs. We identified a galaxy with $L_{IR} > 10^{11}L_{\odot}$ as a LIRG; the final sample of LIRGs has 21 sources. The deep exposure of the UDF allows us to detect their optical counterparts down to low surface brightness, removing potential biases from less-deep classification imagery. The $10\text{-}\sigma$ surface brightness at z -band is $27.52\ \text{arcsec}^{-2}$, which corresponds to a rest-frame B -band surface brightness of 24.5 for a fiducial galaxy at $z=1$. This corresponds well to the typical surface brightness level reached in morphological studies of local galaxies (although at lower physical resolution). It is also close

to the central surface brightness of a local low-surface-brightness (LSB) galaxy. In addition, the LIRG sample is sufficiently large for reliable statistics, as can be seen from the results in Table 2.

We also created a sample of 5 MIPS-detected but lower luminosity non-LIRGs and a control sample of 137 MIPS-non-detected galaxies. The sample of MIPS-detected non-LIRGs is composed of galaxies with $L_{IR} < 10^{11} L_{\odot}$ and $M_B < -18.5$. The sample of MIPS-non-detected galaxies is derived from the sample of 252 normal galaxies with the additional constraints that $M_B < -18.5$ and that the redshift be greater than the minimum redshift of the LIRGs. The cut-off magnitude $M_B = -18.5$ is approximately the rest-frame B magnitude of the faintest LIRG.

Figure 1 shows the redshift distributions of the three samples and the infrared luminosity at $24 \mu\text{m}$ flux density of 0.06 mJy as a function of redshift. Galaxies of all three samples mainly fall at $z > 0.3$. The sample of LIRGs and MIPS-non-detected galaxies have almost the same redshift distributions while non-LIRGs mainly fall at lower redshift due to the detection limits. In the following analysis, we mainly discuss the morphologies of the LIRGs and comparisons to the MIPS-non-detected galaxies, since the MIPS-detected non-LIRGs have a different redshift range and are few in number.

3.2. Quantitative Morphology Classification: Concentration and Asymmetry

Before measuring the concentration and asymmetry value for each galaxy, some image processing was required. We identified and masked contaminating sources in the region of the galaxy using z -band segmentation maps provided with the UDF data release. We replaced the mask region with noise to compute the morphology parameters.

We measured the concentration index using the methodology described in Bershady et al. (2000). To study the morphologies in a fixed-size aperture at the physical scale of each galaxy, the dimensionless parameter η as defined by $\eta(r) = I(r) / \langle I(r) \rangle$ (Petrosian 1976) is used to define the total size of the galaxy, where $I(r)$ is the surface brightness at radius r and $\langle I(r) \rangle$ is the mean surface brightness within radius r . The apparent total magnitudes are then integrated over an aperture equivalent to the total size of the galaxy defined as twice the radius ($\eta = 0.2$). Based on the measured curve of growth, the concentration index is defined by

$$C = 5 \log \frac{r_{80}}{r_{20}}, \quad (1)$$

where r_{80} and r_{20} are the radii that enclose 80% and 20% of the total light (Kent 1985), respectively.

The full description of the algorithm to compute the asymmetry index is in Conselice et al. (2000). The asymmetry parameter is defined as:

$$A = \min\left(\frac{\sum |I_0 - I_{180}|}{\sum |I_0|}\right) - \min\left(\frac{\sum |B_0 - B_{180}|}{\sum |I_0|}\right), \quad (2)$$

where the sums are over the total size of the galaxy as defined above. In the above equation, the first term represents the asymmetry of the galaxy and the second one corrects the effect of noise on the asymmetry measurement, where I_0 and I_{180} are the intensity of each pixel

of the image and of the image rotated by 180° , respectively, and B_0 and B_{180} are the intensity of each pixel of the background region and its 180° -rotated counterpart, respectively. We extracted a 100×100 pixel background region without any contamination and scaled the asymmetry of this region by the relative size of the galaxy to this background region area. The asymmetry minimum was obtained by searching the minimum of asymmetries at rotation centers around the initial galaxy center. See Conselice et al. (2000) for the detailed computation algorithm to locate the rotation center producing the asymmetry minimum.

The uncertainty in the concentration measurement is mainly due to the spatial resolution. Bershady et al. (2000) show that the uncertainty of this parameter is around 0.2 for $r_{50} > 5$ pixel. For asymmetry measurements, the noise of the image is the main effect. Conselice et al. (2000) show that asymmetry measurements have errors around 0.02 for $S/N > 500$ and around 0.05 for $100 < S/N < 300$. We tested our programs by computing the concentration and asymmetry parameters of 20 galaxies in Conselice (2003) with asymmetry spanning from 0.01 to 0.4 and concentration from 2.5 to 4.5. The average differences in concentration and asymmetry parameters are 0.2 and 0.02, respectively. For galaxies with SNR better than 100 in our sample, we estimate the typical errors of the concentration and asymmetry indices are around 0.3 and 0.04, respectively, which are adequate for our study.

4. RESULTS

4.1. Morphologies of a Representative Sample of LIRGs at $0.3 < z < 1.4$

An important aspect of this study is that we can determine morphological properties for a representative sample of high- z LIRGs. In the UDF, 23 of 34 MIPS-detected galaxies at $0.3 < z < 1.4$ with $M_B < -18.5$, $S/N > 100$ and $r_{50} > 5.0$ are LIRGs. Compared with 137 MIPS-non-detected galaxies with the same constraints as above, we find that $\sim 15\%$ of the galaxies with $M_B < -18.5$, $S/N > 100$ and $r_{50} > 5.0$ are LIRGs at $z \sim 1$. This fraction may be underestimated due to the non-detection of LIRGs near $L_{IR} \sim 10^{11} L_{\odot}$ and also may be overestimated as a result of missing non-LIRGs near $M_B = -18.5$ at high redshift. However, the portion of LIRGs in our sample is similar to those found by others at similar redshift. For example, the fraction of LIRGs at $z > 0.4$ in the Canada France Redshift Survey (CFRS) is about 16% without correction for the non-detection of galaxies near the cut-off limits (Hammer et al. 2005). Another test is to use the infrared and optical luminosity functions. Le Floc'h et al. (2005) recently obtained the infrared luminosity function at $0 < z < 1.2$ based on the MIPS/*Spitzer* $24 \mu\text{m}$ sources located in the CDFS. Using $L_{IR}^* = 1.9 \times 10^{10} L_{\odot}$, $\alpha_{IR} = 1.23$ and $\sigma_{IR} = 0.72$ at $1.0 < z < 1.2$, we estimate 70% of the LIRGs at $0.9 < z < 1.4$ are below 0.06 mJy. Using the rest-frame B -band luminosity function of the COMBO-17 survey (Wolf et al. 2003), we estimate 65% of the galaxies with $M_B < -18.5$ are below $m_B = 25$. Correcting the fraction of non-detected galaxies at high redshift, we find that the fraction of LIRGs is almost the same ($\sim 18\%$) as in our study. At $z < 0.9$ where both LIRGs and $M_B < -18.5$ galaxies are detected, we obtain a fraction $\sim 15\%$ of LIRGs for a

total of 67 galaxies. We conclude from all these arguments that the fraction of LIRGs for $M_B < -18.5$ is $\sim 15\%$ at $0.3 < z < 1.4$, the same as in our study. This fraction is much larger than that in the local universe, which is 0.5% for galaxies with $L_{\text{tot}} > 10^{10} L_{\odot}$ (Soifer et al. 1986).

Table 1 lists the LIRGs detected in the UDF along with their concentration and asymmetry indices, C and A . MIPS-4641, MIPS-5117 and MIPS-15236 have X-ray detections (Giacconi et al. 2002) and are classified as type 1 AGN by W. Zheng et al. (2004). These three sources are excluded in our study of morphologies. The other two MIPS sources detected in the X-ray are classified as galaxies by W. Zheng et al. (2004) and are kept in this study.

Table 2 lists the statistical results for LIRGs, non-LIRGs and the MIPS-non-detected sample in the intermediate redshift bin $0.3 < z < 0.9$, in the high redshift bin $0.9 < z < 1.4$, and for the local (low redshift) LIRGs. At $0.3 < z < 0.9$, the $24 \mu\text{m}$ detection limit (0.06 mJy) and the B-band magnitude limit (-18.5) yield complete samples of LIRGs and MIPS-non-detected galaxies, respectively. At $0.9 < z < 1.4$, both the LIRGs and MIPS-non-detected samples are incomplete. We mainly discuss our result based on the complete sample. However, the MIPS-non-detected sample at $0.9 < z < 1.4$ is still dominated by non-LIRGs. Given 9 LIRGs, 88 MIPS-non-detected objects and 70% incompleteness in IR-detection at $0.9 < z < 1.4$, the fraction of LIRGs in 88 MIPS-non-detected objects is $< 25\%$. Therefore, the comparison of morphologies between LIRGs and MIPS-non-detected galaxies at this redshift range is still helpful in our understanding the difference in morphologies between infrared-active galaxies and infrared-inactive galaxies.

Figure 2 shows the rest-frame B-band images for LIRGs used for our morphological study. Figure 3 plots the galaxies along with our other two high- z samples on the C, A plane. The solid curves show the division of this plane into three regions mainly populated by early-type, intermediate-type and late-type galaxies, based on classifications of local galaxies (c.f. Abraham et al. 1996a,b; Conselice et al. 2000). Figure 2 shows that the high-redshift LIRGs are predominantly late-type galaxies (as found previously by Bell et al. 2005a) with asymmetric structures, including long tidal tails and distorted disks. Some of them have very low surface brightness, such as MIPS-5106 with rest-frame B-band surface brightness $\mu_{B0} = 22.4$ within the Petrosian radius.

We define a galaxy with $A > 0.2$ as an asymmetric galaxy in this study. This is motivated by the fact that most ($\sim 90\%$) of local normal galaxies including elliptical galaxies, early-type (Sa-Sb) and late-type spiral galaxies (Sc-Sd), have asymmetry $A < 0.2$ (Conselice 2003). As listed in Table 2, $90_{-30}^{+10}\%$ of the LIRGs in the UDF are late-type galaxies and $80 \pm 10\%$ of the LIRGs are asymmetric ($A > 0.2$) objects.

The classification of the high- z galaxies using the asymmetry and concentration indices is generally consistent with the conventional visual classifications. Figure 2 shows that only two sources, MIPS-5115 and MIPS-13901 are classified visually differently from the results using the structural parameters. In this paper, we make no use of the conventional classifications (other than to

place some results in context), basing all of our conclusions on the CA analysis. Thus, the small number of classification discrepancies has no effect on our conclusions.

4.2. Comparison of LIRG Morphologies to those of MIPS-non-detected Galaxies

In this Section, we compare the morphologies of LIRGs in the UDF to those of MIPS-non-detected galaxies. Table 2 shows that the correlations at high redshift between infrared luminosity and morphology are weak. On average, high- z LIRGs are more asymmetric than the MIPS-non-detected galaxies, characterized by a higher fraction of $A > 0.35$ (merging; Conselice 2003) galaxies and fewer symmetric objects, defined as $A < 0.2$. However, a number of MIPS-non-detected galaxies show asymmetric structures and/or are currently involved in merging activity. In the following we compare the morphological distributions in terms of the fraction of late-type galaxies and the distribution of asymmetry parameters.

4.2.1. Distributions of the Asymmetry and Concentration Parameters

Table 2 lists the average asymmetries and the standard deviations of the means. The LIRGs have asymmetry around 0.34, somewhat higher than $A = 0.22$ of the MIPS-non-detected galaxies. The K-S test shows the probabilities that LIRGs and MIPS-non-detected galaxies have the same distribution of asymmetries are 1% and $< 0.1\%$ for the intermediate-redshift and high-redshift bins, respectively. This seems consistent with the suggestion (e.g. Larson & Tinsley 1978; Sanders & Mirabel 1996; Barton et al. 2000) that non-symmetric structures, such as tidal distortions, companions, and distorted disks, play an important role in enhancing star formation in galaxies. Figure 3 indicates that the MIPS-non-detected galaxies have a wide distribution of morphologies, from classical Hubble types to highly asymmetric, most likely merging systems. The fraction of symmetric ($A < 0.2$) galaxies in this sample is high ($\sim 50\%$). In comparison, the LIRGs virtually lack symmetric objects ($\sim 10\%$).

As listed in Table 2, the sample of LIRGs shows a slightly higher fraction of late-type galaxies than the sample of MIPS-non-detected galaxies, although the values are consistent within statistical errors. The classification calibration method in this comparison is based on visually classified local galaxies (Conselice et al. 2000). Alternatively, Cassata et al. (2005) measured the rest-frame B morphology for the K-band selected high-redshift galaxies and used the boundary ($A < 0.2$ and $C > 2.9$) to define the early-type galaxies. Based on their method, we find that the late-type fraction of LIRGs is still a little higher at $0.3 < z < 1.5$, i.e., the $24 \mu\text{m}$ -selected sample is biased a little toward late-type galaxies. However, much of this relatively minor difference can be explained by the larger portion of symmetric early- and intermediate-type galaxies in the MIPS-non-detected sample. The differences in morphologies between the late-type galaxies of these two samples are therefore minor.

On the other hand, the galaxies of both samples are more asymmetric than the local Hubble-type galaxies and even slightly more asymmetric than the non-starburst local dwarf irregular galaxies, which have

asymmetry of 0.17 ± 0.10 (Conselice 2003). The K-S test shows that the probability that LIRGs and local irregular galaxies have the same distribution of asymmetry is $< 0.1\%$, while such a probability for MIPS-non-detected galaxies at $0.3 < z < 0.9$ and local irregular galaxies is 27%. Conselice et al. (2000) show that low spatial resolution affects the asymmetry measurement by making the galaxy appear more symmetric. The spatial resolutions are 50 pc/pixel for the local sample of Conselice (2003) and 300 pc/pixel for our galaxies at $z=0.5$. This reinforces our conclusion that the galaxies in the UDF are more asymmetric than the local galaxies.

Although the two high- z samples show somewhat different levels of asymmetry, their concentrations are almost the same, characterized by values that are comparable to the local late-type disk-galaxies (Sc-Sd; Conselice 2003). The K-S test shows that the LIRG sample and the MIPS-non-detected sample have the same distribution of concentration with a probability of 40% and 30% in the intermediate and high redshift bins, respectively. Conselice (2003) argues that the concentration index reveals the past star-formation history of a galaxy because of the correlation of bulge to total light ratios and stellar masses with this index. This behavior implies that the MIPS-non-detected galaxies have similar stellar populations and distributions as the LIRGs except for the LIRGs having a large population of massive young stars due to the presence of a starburst.

4.2.2. Merging Galaxies

It is also of interest to determine how many LIRGs are merging. We classify an object as a merger if its asymmetry parameter is greater than 0.35 (Conselice 2003). The merger as defined here means a major merger, i.e., that the two progenitor galaxies have comparable masses. However, other strong asymmetries may also satisfy this numerical definition. By this definition, the LIRG sample is composed of $40 \pm 20\%$ merging systems, higher than the merging fraction ($\sim 15\%$) of the MIPS-non-detected sample. Although the merging fraction obtained by the asymmetry technique depends on the A value used for merger identification, this conclusion does not change with modest changes in this defining value of A .

Our sample shows 40% of LIRGs at $0.3 < z < 1.4$ are merging systems as identified by the CA method (which emphasizes high levels of morphological disturbance in systems with high surface brightness). This result is probably consistent with but higher than that of Bell et al. (2005a) who found that less than 30% of 1500 star-forming galaxies at redshift $0.65 < z < 0.75$ are strongly interacting based on visual classifications, and that of W. Zheng et al. (2004) who found that 6 ($\sim 17\%$) of 36 distant ($z \gtrsim 0.4$) LIRGs in the CFRs are obvious ongoing major mergers. W. Zheng et al. (2004) do not count the irregular galaxies (22%), which may have $A > 0.35$, as merging galaxies. Another cause for these differences is that the morphologies of a merging galaxy at different surface brightness levels show different levels of asymmetry and thus visual identification on a relatively shallow image may mis-classify it as a non-merging galaxy.

5. DISCUSSION

5.1. Continuous Morphological Transformation plus Episodic Starbursts

Our study of morphologies and infrared properties of high-redshift galaxies in the UDF has two basic results. The first one is that LIRGs and MIPS-non-detected galaxies in the UDF are predominantly late-type asymmetric galaxies. The LIRGs are somewhat more asymmetric on average than MIPS-non-detected galaxies and they are characterized by a higher fraction of very asymmetric ($A \geq 0.35$) systems and a lower fraction of symmetric ($A < 0.2$) objects. This result is consistent with the proposal that non-symmetric structures play an important role in enhancing the star formation and hence elevate the infrared luminosities of galaxies. The second result is that there is no one-to-one correlation between the occurrence of high infrared luminosities and disturbed morphologies: highly asymmetric galaxies, including merging systems, do not necessarily have high infrared luminosities.

On average, high- z LIRGs and normal galaxies are both more asymmetric than local irregular types, and their concentration indices are similar to the local late-type disk galaxies. Are the asymmetric normal galaxies and the LIRGs two different populations or are they the same population but in different stages? That is, are the activities of starbursts episodic so that the LIRGs are now in active stages and asymmetric non-LIRGs are similar galaxies that are in quiescent states between-starburst stages?

Based on the statistics at $0.3 < z < 0.9$ listed in table 2, 25% of asymmetric galaxies ($A > 0.2$) are LIRGs at $0.3 < z < 0.9$. This fraction is $\sim 10\%$ in the local universe, assuming a merging fraction of 4% (Marzke et al. 1998), a LIRG fraction of 0.5% (Soifer et al. 1986) and an asymmetric galaxy fraction in LIRGs of 74% based on the fraction of close pair and strongly interacting galaxies (Sanders et al. 1988). One candidate population for asymmetric galaxies without starbursts is interacting galaxies with low metallicity and hence low dust. However, Kobulnicky & Kewley (2004) find that the shift of the luminosity-metallicity relation is smaller than 27% at $z \sim 1.0$ compared to the local trend, based on the nebular emission lines of galaxies ($18.5 < M_B < -21.5$) with $SFR \sim 0.1-10 M_{\odot} yr^{-1}$. This result is consistent with previous studies (Kobulnicky & Zaritsky 1999; Carollo & Lilly 2001). We conclude that both LIRGs and MIPS-non-detected galaxies are not likely to be extremely deficient of dust. Another candidate population for asymmetric non-detected galaxies is interacting galaxies without gas, e.g., interactions between galaxies composed entirely of stars. However, such "dry mergers" appear in general to be uncommon ($\sim 1\%$) (Bell et al. 2005b). Therefore, the similar distributions of concentration index for LIRGs and asymmetric non-MIPS-detected galaxies suggests that these two samples have similar formation histories. The moderately higher asymmetry for the LIRGs could arise from luminous off-nuclear star formation, or from extinction. Thus, the elevated periods of star formation are probably occurring episodically.

In the local universe, starbursts in a given galaxy have a short duration of 0.01 to 0.07 Gyr (Krabbe et al. 1994; Lutz et al. 1996; Alonso-Herrero et al. 2000).

Near-IR imaging and spectroscopy in the starburst galaxies M82, IC 342 and NGC 253 indicate several episodes of enhanced star formation (Rieke et al. 1993; Satyapal et al. 1997; Böker et al. 1997; Engelbracht et al. 1998; Förster Schreiber 2000). The anticorrelation between equivalent width of H α and galaxy pair spatial separation found by Barton et al. (2000) indicates that the starburst episodes are initiated by a series of close passes. In the early Universe, Lyman Break Galaxies (LBGs) show comparable durations of starburst activity (Papovich et al. 2001; Shapley et al. 2005). Recently, Yan et al. (2004) and Papovich et al. (2005) found that the broadband photometry data for massive galaxies at $z \sim 1-3$ are better fit by a model star-formation history with recent bursts superimposed on an underlying stellar population compared to simple, monotonically-evolving stellar populations. They conclude that these galaxies have a complicated history with many episodes of star formation. Theoretically, simulations show that in merging galaxies, strong gas inflow is triggered and nuclear star formation is ignited only after enough gas is accumulated in the center of the galaxies (e.g. Noguchi 1991; Mihos et al. 1993; Barnes & Hernquist 1996). During the whole merging process, strong enhancement of the star formation only occurs with a short duration, which supports the proposal for episodic starbursts. A star formation history involving episodic events is also indicated by recent semi-analytic studies (e.g. Somerville et al. 2001; Nagamine et al. 2005).

Given the merging timescale t_{merge} , the fraction f of t_{merge} at which galaxies are actually involved in starbursts, and the timescale for episodic starbursts t_{ESB} , we can estimate the total number of episodes during one merging event $N_{\text{ESB}} = f \times t_{\text{merge}} / t_{\text{ESB}}$. We adopt 0.5 Gyr for the timescale of the greatest merger activity (e.g. Patton et al. 2000). The characteristic timescale of starbursts is estimated at 10-70 Myr as shown above. The fraction f can be computed from the merging fractions of LIRGs and infrared-inactive galaxies as listed in Table 1 and the fraction of LIRGs in a given magnitude-limited sample. We adopt 15% as the fraction of LIRGs as shown in Section 4.1 and find $f = 0.15 \times 0.4 / (0.15 \times 0.4 + 0.85 \times 0.16) = 0.3$. Therefore, the average number of episodes during a merging event is around 4 for $t_{\text{ESB}} = 0.04$ Gyr. This indicates that during each merging event, at least one episode of vigorous star formation can be triggered and multiple episodes of such activity are possible.

This conclusion is supported by the studies of nearby galaxies cited above. In addition, simulations by Mihos & Hernquist (1996) show that during merging events, bulgeless disc galaxies can trigger gas inflow even before the occurrence of the actual collision of the galaxies and thus two starburst episodes can occur during the merging event. Recently, Tissera et al. (2002) has shown that in hierarchical clustering scenarios, some merging events can have two episodes of starbursts: one owing to the gas inflow driven as the satellite approaches, and the second one occurring in the collisions of baryonic clumps.

5.2. Comparisons to the Local LIRGs

In the last column of Table 2, we present the statistical results for local LIRGs listed in the IRAS Bright Galaxy Sample (Soifer et al. 1987). We extracted the image for

each source from the Digitized Sky Survey (DSS) at the POSS2/UKSTU blue band. The table shows that the morphologies of local LIRGs are similar to those of the MIPS-non-detected sample and the LIRGs in the UDF in terms of the fraction of late-type galaxies, of merging galaxies and of symmetric galaxies. The mean asymmetry and concentration of LIRGs in the UDF are slightly higher than those of local LIRGs. The K-S test shows that the probability that the LIRGs at $0.3 < z < 0.9$ and local LIRGs have the same distribution of asymmetry and concentration are 3% and 9%, respectively. That is, the apparent differences are only marginally significant. In the local universe, a very low (4%) fraction of the total population is irregular and interacting galaxies (Marzke et al. 1998). As a result, the morphologies of local LIRGs are quite different from the local normal infrared-inactive galaxies, which is not the case at high-redshift. The small difference in the morphologies between LIRGs and infrared-inactive galaxies in the UDF is due to the fact that, at high redshift, a significant fraction of galaxies are asymmetric systems in which starbursts are much more easily triggered. Locally, LIRGs are exceptional, and an exceptional disturbance is required to trigger their elevated rates of star formation. Based on this trend, we can expect that at higher redshift ($z > 1.5$), the morphologies of LIRGs and non-LIRGs will be even more indistinguishable.

The similarity between the morphologies of local and high- z LIRGs suggests that a certain level of asymmetry is correlated with vigorous star formation, independent of redshift. This situation probably arises because once star formation is initiated, it evolves within a galaxy independent of the galaxy environment (Balogh et al. 2004). Therefore, a similar level of perturbation leads to similar consequences in terms of elevated star formation. At $z \sim 1$, most galaxies appear to have an appropriate level of asymmetry potentially to be transformed into LIRGs by relatively minor mergers. Therefore, the incidence of LIRGs is high, leading to a high density of star formation. Locally, most galaxies are highly symmetric and only exceptional circumstances, such as an interaction with another massive galaxy, can produce the situations that are a prerequisite for a LIRG. Hence, the incidence of LIRGs is low and so is the density of star formation.

6. CONCLUSIONS

In this paper, we have investigated the morphologies of 18 high-redshift ($0.3 < z < 1.4$) LIRGs in the UDF down to a rest-frame B-band surface brightness of $\mu_{B0} = 24.5$. They are a representative sample of the LIRGs that dominate the star formation density at $z \sim 1$. We compare their morphologies to those of MIPS-non-detected galaxies at similar redshift and of 49 local LIRGs. We used the concentration and asymmetry indices to quantify the morphologies of all these galaxies. Our main results are:

(1) The fraction of LIRGs for $M_B < -18.5$ galaxies at this redshift range is around 15%, much higher than the 0.5% in the local universe. Their morphologies are dominated by late-type galaxies with asymmetric ($A > 0.2$) structures and include a significant number that appear to be mergers ($40 \pm 20\%$). The morphologies of LIRGs in the UDF are similar to those of local LIRGs but possibly somewhat more asymmetric. Optically luminous MIPS-non-detected galaxies at $z \sim 1$ are nearly as asym-

metric as LIRGs, in contrast to the local universe where infrared-inactive galaxies are far more symmetric than local LIRGs.

(2) All of the high- z galaxy types are relatively asymmetric, more so than even local irregular types. Their concentration indices are similar to those of local late-type disk galaxies. We argue that the asymmetric LIRGs and asymmetric MIPS-non-detected galaxies are from the same parent population but in different stages of star formation, which suggests the star formation is episodic. Under this hypothesis, the fraction of the duration of the IR-active phase for asymmetric ($A > 0.2$) galaxies is $\sim 25\%$.

(3) The morphologies of local LIRGs and LIRGs at $z \sim 1$ are similar, suggesting that similar conditions within the galaxy lead to LIRG-levels of star formation. At $z \sim 1$, such conditions are common and LIRGs

can develop by relatively minor mergers. Locally, most galaxies are highly symmetric, and only exceptional circumstances such as an interaction with another massive galaxy can create the level of asymmetry associated with LIRG-levels of star formation.

7. ACKNOWLEDGEMENTS

We thank the anonymous referee for very detailed and constructive comments. We also thank John Moustakas, Jennifer Lotz, Lei Bai, Amy Stutz, Linhua Jiang and Jun Cui for helpful discussions. This study depended on the publicly released products from the HST Ultradeep Field. Support for this work was provided by NASA through contract 1255094 issued by JPL/California Institute of Technology.

REFERENCES

- Abraham, R. G., Valdes, F., Yee, H. K. C., & van den Bergh, S. 1994, *ApJ*, 432, 75
- Abraham, R. G., Tanvir, N. R., Santiago, B. X., Ellis, R. S., Glazebrook, K., & van den Bergh, S. 1996a, *MNRAS*, 279, L47
- Abraham, R. G., van den Bergh, S., Glazebrook, K., Ellis, R. S., Santiago, B. X., Surma, P., & Griffiths, R. E. 1996b, *ApJS*, 107, 1
- Alonso-Herrero, A., Rieke, G. H., Rieke, M. J., & Scoville, N. Z. 2000, *ApJ*, 532, 845
- Armus, L., Heckman, T., & Miley, G. 1987, *AJ*, 94, 831
- Balogh, M. L., Baldry, I. K., Nichol, R., Miller, C., Bower, R., & Glazebrook, K. 2004, *ApJ*, 615, L101
- Barnes, J. E., & Hernquist, L. 1996, *ApJ*, 471, 115
- Barton, E. J., Geller, M. J., & Kenyon, S. J. 2000, *ApJ*, 530, 660
- Beckwith, S. V., et al. 2005, in preparation
- van den Bergh, S. 1960a, *ApJ*, 131, 558
- van den Bergh, S. 1960b, *ApJ*, 131, 215
- Bell, E. F., et al. 2005a, *ApJ*, 625, 23
- Bell, E. F. et al. 2005b, arXiv:astro-ph/0506425
- Bershady, M. A., Jangren, A., & Conselice, C. J. 2000, *AJ*, 119, 2645
- Bertin, E., & Arnouts, S. 1996, *A&AS*, 117, 393
- Blanton, M. R., et al. 2003, *AJ*, 125, 2348
- Böker, T., Forster-Schreiber, N. M., & Genzel, R. 1997, *AJ*, 114, 1883
- Brinchmann, J., et al. 1998, *ApJ*, 499, 112
- Carollo, C. M., & Lilly, S. J. 2001, *ApJ*, 548, L153
- Cassata, P., et al. 2005, *MNRAS*, 357, 903
- Conselice, C. J., Bershady, M. A., & Jangren, A. 2000, *ApJ*, 529, 886
- Conselice, C. J. 2003, *ApJS*, 147, 1
- Conselice, C. J., Blackburne, J. A., & Papovich, C. 2005, *ApJ*, 620, 564
- Cutri, R. M., & McAlary, C. W. 1985, *ApJ*, 296, 90
- Driver, S. P., Fernandez-Soto, A., Couch, W. J., Odewahn, S. C., Windhorst, R. A., Phillips, S., Lanzetta, K., & Yahil, A. 1998, *ApJ*, 496, L93
- Driver, S. P., Windhorst, R. A., & Griffiths, R. E. 1995, *ApJ*, 453, 48
- Ellis, R. S., Colless, M., Broadhurst, T., Heyl, J., & Glazebrook, K. 1996, *MNRAS*, 280, 235
- Elmegreen, D. M., Elmegreen, B. G., Rubin, D. S., & Schaffer, M. A. 2005, *ApJ*, 631, 85
- Engelbracht, C. W., Rieke, M. J., Rieke, G. H., Kelly, D. M., & Achtermann, J. M. 1998, *ApJ*, 505, 639
- Fazio, G. G., et al. 2004, *ApJS*, 154, 10
- Förster Schreiber, N. M. 2000, *New Astronomy Review*, 44, 263
- Giacconi, R., et al. 2002, *ApJS*, 139, 369
- Gordon, K. D., et al. 2005, *PASP*, 117, 503
- Hammer, F., Flores, H., Elbaz, D., Zheng, X. Z., Liang, Y. C., & Cesarsky, C. 2005, *A&A*, 430, 115
- Hopkins, A. M. 2004, *ApJ*, 615, 209
- Huang, J.-S., et al. 2004, *ApJS*, 154, 44
- Hubble, E. P. 1926, *ApJ*, 64, 321
- Hubble, E. P. 1936, Yale University Press,
- Kennicutt, R. C. 1998, *ARA&A*, 36, 189
- Kent, S. M. 1985, *ApJS*, 59, 115
- Kleinmann, S. G., Hamilton, D., Keel, W. C., Wynn-Williams, C. G., Eales, S. A., Becklin, E. E., & Kuntz, K. D. 1988, *ApJ*, 328, 161
- Kobulnicky, H. A., & Kewley, L. J. 2004, *ApJ*, 617, 240
- Kobulnicky, H. A., & Zaritsky, D. 1999, *ApJ*, 511, 118
- Krabbe, A., Sternberg, A., & Genzel, R. 1994, *ApJ*, 425, 72
- Lagache, G., et al. 2004, *ApJS*, 154, 112
- Larson, R. B., & Tinsley, B. M. 1978, *ApJ*, 219, 46
- Le Floc'h, E., Charmandaris, V., Laurent, O., Mirabel, I. F., Gallais, P., Sauvage, M., Vigroux, L., & Cesarsky, C. 2002, *A&A*, 391, 417
- Le Floc'h, E., et al. 2005, *ApJ*, 632, 169
- Le Fèvre, O., et al. 2004, *A&A*, 428, 1043
- Lilly, S. J., Le Fevre, O., Crampton, D., Hammer, F., & Tresse, L. 1995, *ApJ*, 455, 50
- Lutz, D., et al. 1996, *A&A*, 315, L137
- Mann, R. G., et al. 1997, *MNRAS*, 289, 482
- Marzke, R. O., da Costa, L. N., Pellegrini, P. S., Willmer, C. N. A., & Geller, M. J. 1998, *ApJ*, 503, 617
- Melbourne, J., Koo, D. C., & Le Floc'h, E. 2005, *ApJ*, 632, L65
- Menanteau, F., Ford, H. C., Motta, V., Benitez, N., Martel, A. R., Blakeslee J. P., & Infante L. 2005, astro-ph/0509759
- Mihos, J. C., Bothun, G. D., & Richstone, D. O. 1993, *ApJ*, 418, 82
- Mihos, J. C., & Hernquist, L. 1996, *ApJ*, 464, 641
- Nagamine, K., Cen, R., Hernquist, L., Ostriker, J. P., & Springel, V. 2005, *ApJ*, 618, 23
- Noguchi, M. 1991, *MNRAS*, 251, 360
- Okamura, S., Kodaira, K., & Watanabe, M. 1984, *ApJ*, 280, 7
- Papovich, C., Dickinson, M., & Ferguson, H. C. 2001, *ApJ*, 559, 620
- Papovich, C., & Bell, E. F. 2002, *ApJ*, 579, L1
- Papovich, C., Giavalisco, M., Dickinson, M., Conselice, C. J., & Ferguson, H. C. 2003, *ApJ*, 598, 827
- Papovich, C., et al. 2004, *ApJS*, 154, 70
- Papovich, C., et al. 2005, astro-ph/0511289
- Patton, D. R., Carlberg, R. G., Marzke, R. O., Pritchett, C. J., da Costa, L. N., & Pellegrini, P. S. 2000, *ApJ*, 536, 153
- Pérez-González, P. G., et al. 2005, *ApJ*, 630, 82
- Petrosian, V. 1976, *ApJ*, 209, L1
- Rieke, G. H., Loken, K., Rieke, M. J., & Tamblyn, P. 1993, *ApJ*, 412, 99
- Rieke, G. H., et al. 2004, *ApJS*, 154, 25
- Roberts, M. S., & Haynes, M. P. 1994, *ARA&A*, 32, 115
- Sandage, A. R. 1961, *The Hubble Atlas of Galaxies* (Washington: Carnegie Inst. Washington)
- Sandage, A., & Tammann, G. A. 1987, *A revised Shapley-Ames Catalog of Bright Galaxies* (Washington: Carnegie Inst. Washington)
- Sandage, A., & Bedke, J. 1994, *Carnegie Atlas of Galaxies* (Washington: Carnegie Inst. Washington)
- Sanders, D. B., Soifer, B. T., Elias, J. H., Madore, B. F., Matthews, K., Neugebauer, G., & Scoville, N. Z. 1988, *ApJ*, 325, 74

- Sanders, D. B., & Mirabel, I. F. 1996, *ARA&A*, 34, 749
- Satyapal, S., Watson, D. M., Pipher, J. L., Forrest, W. J., Greenhouse, M. A., Smith, H. A., Fischer, J., & Woodward, C. E. 1997, *ApJ*, 483, 148
- Shapley, A. E., Steidel, C. C., Erb, D. K., Reddy, N. A., Adelberger, K. L., Pettini, M., Barmby, P., & Huang, J. 2005, *ApJ*, 626, 698
- Somerville, R. S., Primack, J. R., & Faber, S. M. 2001, *MNRAS*, 320, 504
- Soifer, B. T., et al. 1984, *ApJ*, 278, L71
- Soifer, B. T., Sanders, D. B., Neugebauer, G., Danielson, G. E., Lonsdale, C. J., Madore, B. F., & Persson, S. E. 1986, *ApJ*, 303, L41
- Soifer, B. T., Sanders, D. B., Madore, B. F., Neugebauer, G., Danielson, G. E., Elias, J. H., Lonsdale, C. J., & Rice, W. L. 1987, *ApJ*, 320, 238
- Steidel, C. C., Adelberger, K. L., Giavalisco, M., Dickinson, M., & Pettini, M. 1999, *ApJ*, 519, 1
- Thompson, R. I., et al. 2005, *AJ*, 130, 1
- Tissera, P. B., Domínguez-Tenreiro, R., Scannapieco, C., & Sáiz, A. 2002, *MNRAS*, 333, 327
- Vanzella, E., et al. 2005, *A&A*, 434, 53
- de Vaucouleurs, G. 1959, *Handbuch der Physik*, 53, 311
- Windhorst, R. A., et al. 2002, *ApJS*, 143, 113
- Wolf, C., Meisenheimer, K., Rix, H.-W., Borch, A., Dye, S., & Kleinheinrich, M. 2003, *A&A*, 401, 73
- Wolf, C., et al. 2004, *A&A*, 421, 913
- Yan, H., et al. 2004, *ApJ*, 616, 63
- Zheng, X. Z., Hammer, F., Flores, H., Assémat, F., & Pelat, D. 2004, *A&A*, 421, 847
- Zheng, W., et al. 2004, *ApJS*, 155, 73

TABLE 1
LIRGS IN THE UDF WITH UNAMBIGUOUS OPTICAL COUNTERPART

MIPS (1)	RA (2)	DEC (3)	ACS (4)	Sep(") (5)	redshift (6)	f_{24} (mJy) (7)	m_z (8)	A (9)	C (10)	Type (11)	X-ray (12)	z Source (13)
4641	03 32 35.963	-27 48 50.33	566.	0.16	1.31	0.06±0.012	21.56	0.21	3.54	Intermediate	1.31;XID-100	Spec
4644	03 32 37.512	-27 48 38.67	706.	0.41	0.67	0.11±0.013	20.87	0.47	2.51	Late/Interacting		Spec
4645	03 32 37.172	-27 48 33.74	944.	0.21	0.85	0.17±0.015	23.57	0.49	3.19	Late/Interacting		Spec
4649	03 32 41.078	-27 48 53.07	391.	0.09	0.68	0.14±0.012	20.21	0.31	3.41	Late		Spec
5088	03 32 35.564	-27 46 27.35	5628.	1.32	1.08	0.20±0.018	21.12	0.49	2.46	Late/Interacting		36689;21.7
5092	03 32 34.863	-27 46 41.52	6139.	1.08	1.10	0.17±0.016	22.73	0.41	2.91	Late/Interacting		Spec
5096	03 32 38.491	-27 47 2.39	4286.	0.09	0.92/0.97	0.07±0.011	21.19	0.27	3.80	Intermediate		This work/35195,23.0
5104	03 32 39.865	-27 47 15.04	3739.	0.25	1.10	0.16±0.013	21.47	0.27	2.35	Late		Spec
5106	03 32 36.931	-27 47 26.74	3285.	0.57	1.34/0.98	0.14±0.012	23.24	0.41	4.15	Early/Interacting		This work/34336,23.68
5114	03 32 38.767	-27 47 32.24	3062.	0.16	0.46	0.76±0.027	20.88	0.27	3.06	Late	0.46;XID-567	Spec
5115	03 32 37.618	-27 47 43.43	2505.	0.74	1.17/1.06	0.09±0.012	22.11	0.29	3.36	Late		This work/33813,22.85
5117	03 32 39.075	-27 46 1.84	6645.	0.12	1.22	0.26±0.016	20.97	0.07	2.90	Late	1.22;XID-28	Spec
5121	03 32 40.777	-27 46 16.01	5300.	0.32	0.55	0.14±0.013	20.15	0.27	2.44	Late		This work
5628	03 32 43.227	-27 47 56.48	1802.	0.54	0.67	0.16±0.015	20.68	0.20	3.14	Late		Spec
5630	03 32 42.275	-27 47 45.99	2344.	0.16	1.00	0.22±0.015	21.25	0.42	1.79	Late/Interacting		Spec
5768	03 32 31.419	-27 47 25.04	3246.	0.82	0.67	0.12±0.010	21.02	0.46	2.72	Late/Interacting		Spec
5828	03 32 39.217	-27 45 32.16	6930.	0.63	1.04	0.16±0.013	21.84	0.47	3.09	Late/Interacting		Spec
13901	03 32 44.198	-27 47 32.70	2874.	0.86	0.74	0.24±0.020	21.42	0.31	3.24	Late		Spec
15236	03 32 36.533	-27 46 30.66	5761.	1.69	0.71	0.28±0.015	21.21	0.58	2.54	Late/Interacting	0.77;XID-511	36462;21.4
15942	03 32 44.851	-27 47 27.62	2686.	0.15	0.44	0.77±0.044	18.42	0.25	3.11	Late		Spec
15943	03 32 45.103	-27 47 24.24	3382.	0.24	0.44	0.51±0.042	20.41	0.38	2.99	Late/Interacting	0.44;XID-646	Spec

NOTE. — Column (1): The MIPS ID of the LIRGs in the UDF. Column(2): RA of MIPS source. Column(3): DEC of MIPS source. Column(4): ACS ID of optical counterpart of MIPS source. Column(5): The separation in arcsec between ACS source and MIPS source. Column(6): The redshift. Column(7): 24 μ m flux. Column(8): z-band magnitude. Column(9): Asymmetry. Column(10): Concentration. Column(11): The galaxy type of MIPS source based on CA system. Column 12: The photometric redshift and the catalog number of X-ray counterparts of MIPS sources based on the CDFS 1 MS catalog by W. Zheng et al. (2004). Column 13: Where redshifts are from COMBO-17, the corresponding catalog number along with the magnitude at R band is listed; 'This work' indicates that the redshift is computed based on our photo-z code (Pérez-González et al. 2005). 'Spec' means the spectroscopic redshift from VLT/FORS2 spectroscopy catalog (Vanzella et al. 2005) and VIMOS VLT Deep Survey (VVDS) v1.0 catalog (Le Fèvre et al. 2004).

TABLE 2
THE STATISTICS OF MORPHOLOGIES OF $M_B < -18.5$ GALAXIES IN THE UDF AND LOCAL LIRGS

	0.3<z<0.9			0.9<z<1.4		Local LIRGs
	LIRGs	non-LIRGs	Non-detected sample	LIRGs	Non-detected sample	
Total number	10	5	49	8	88	49
Late-type	90±30%	80±40%	78±13%	75±31%	81± 10%	89±14%
Merging (A>0.35)	40±20%	20±20%	16± 6%	63±28%	10± 3%	31± 8%
Symmetric (A<0.2)	10±10%	60±35%	47± 10%	13±13%	65± 9%	43± 9%
A ¹	0.34±0.03	0.22±0.05	0.22±0.02	0.38±0.03	0.18±0.02	0.26±0.03
C ¹	2.98±0.10	3.09±0.11	2.98±0.08	2.99±0.28	2.88±0.05	2.74±0.08

NOTE. — ¹Averages with standard errors of the mean. At the 0.3<z<0.9, both LIRG and MIPS-non-detected samples are complete. At the 0.9<z<1.4, both sample are incomplete.

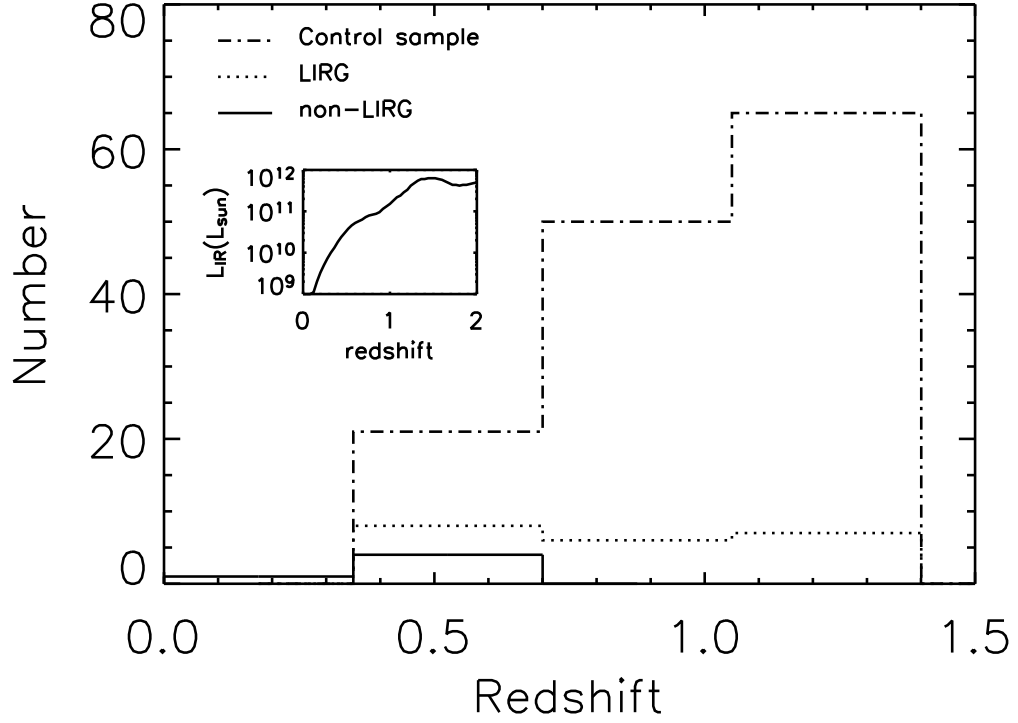


FIG. 1.— The redshift distributions of LIRG ($L_{IR}(8-1000\mu\text{m}) > 10^{11}L_{\odot}$), non-LIRG ($L_{IR}(8-1000\mu\text{m}) < 10^{11}L_{\odot}$) and MIPS-non-detected control samples. The dot-dashed histogram indicates the control sample, the dotted histogram indicates the LIRGs and the solid histogram indicates the non-LIRGs. The control and LIRG samples have almost the same redshift distributions, while non-LIRGs are mainly at low redshift due to the detection limit. The inserted plot shows the IR luminosity at the $24\mu\text{m}$ detection limit (0.06 mJy) as a function of the redshift.

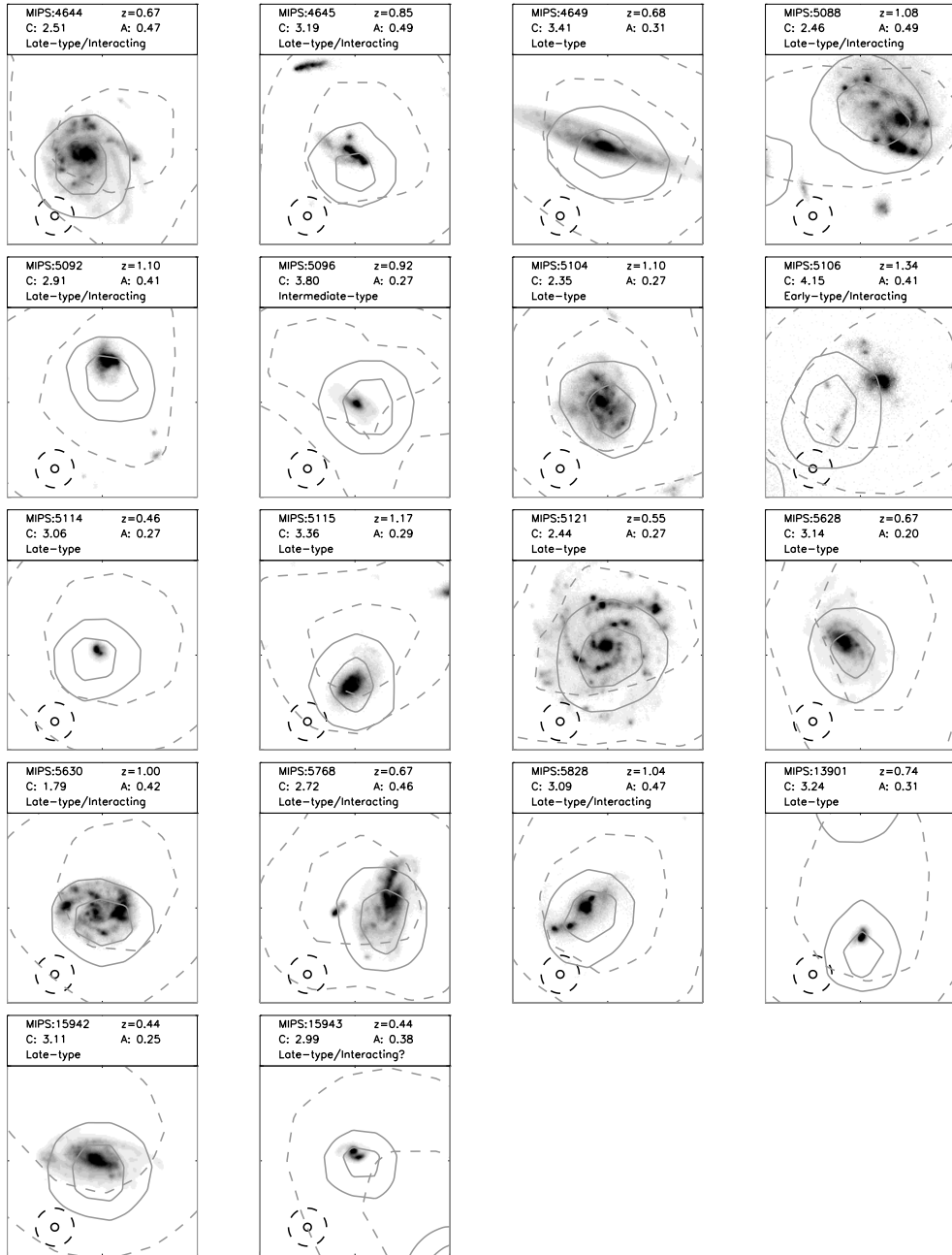


FIG. 2.— The rest-frame B-band images (5×5 arcsec) of non-X-ray LIRGs in the UDF along with the redshifts, structural parameters and the galaxy types based on the CA classification scheme. The center of the image is the position of the MIPS source. The light solid and dashed curves show contours at 20% and 50% enclosing flux for IRAC and MIPS, respectively. The heavy solid and dashed circles show the position accuracy for IRAC sources (0.1 arcsec) and MIPS sources (0.5 arcsec).

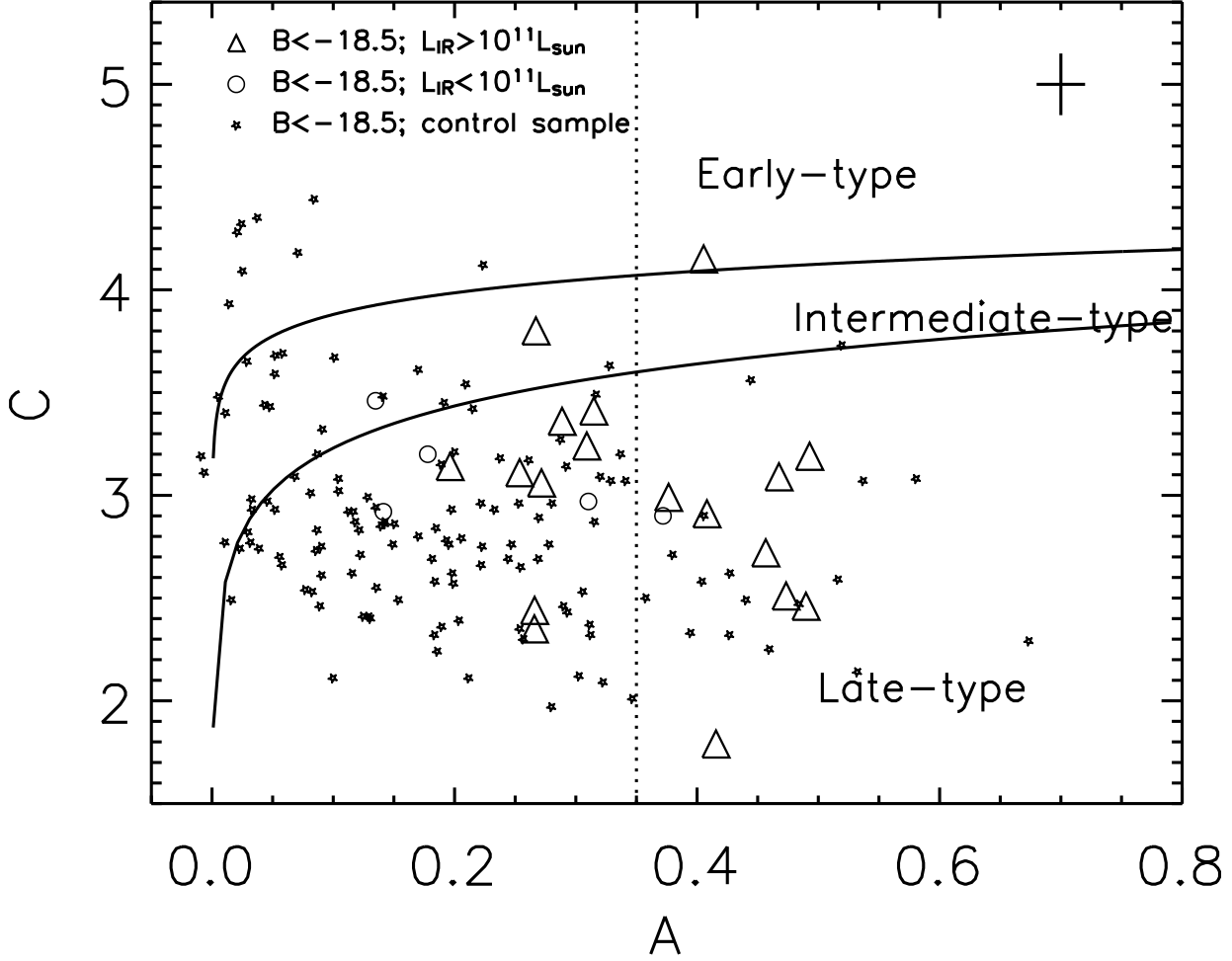


FIG. 3.— The distributions of LIRGs (triangles), non-LIRGs (open circles) and MIPS-non-detected control sample galaxies (stars) in the plane of concentration and asymmetry. The two solid curves divide the plane into three regions populated by early-, intermediate- and late-type galaxies. The dotted line indicates $A = 0.35$, to the right of which galaxies are identified as merging systems. The cross shows typical errors of concentration (0.3) and asymmetry (0.04).